Numerical modeling of reinforced unpaved roads by geogrid

Sadok Benmebarek*, Mohamed Saddek Remadna and Lamine Belounar

Biskra University, Numerical Modelling and Instrumentation Laboratory, Algeria
*benmebareks@yahoo.fr

Abstract: In this paper, numerical computations using Flac software are carried out to investigate the improvement of the bearing capacity of a reinforced unpaved roadway over soft clay. Placed between the subgrade and base course, or within the base course, the geosynthetic improves the performance of unpaved roads carrying channelized traffic and unpaved areas subjected to random traffic. The present study focuses on the mechanisms by which the reinforcement improves the behavior of the roadway under the effect of a static single load. The loading of the road is carried out by imposed displacement of the load contact until reaching a final displacement called rut. The pressure-displacement behavior was determined for small and large strain analysis for unpaved roads with or without reinforcement. The analysis of the distribution and the importance of tangential and normal stresses on the soil-base interface provide an explanation to the effect of the reinforcement in the improvement of the bearing capacity or what is commonly called mechanism of reinforcement. The study also highlights the effect of the stiffness and the anchorage length of the geogrid on the reinforcement.
.

Key words: Modeling, unpaved road, reinforcement, large strain, geogrid.

Introduction

Geosynthetics have been used for subgrade stabilization and base course reinforcement for construction of unpaved roads since the 1970s. Placed between the subgrade and base course, or within the base course, the geosynthetic improves the performance of unpaved roads carrying channelized traffic and unpaved areas subjected to random traffic. Two types of geosynthetics are typically used in unpaved structures: geotextiles and geogrids. From the viewpoint of un-paved structure reinforcement, there is a significant difference between geogrids and geotextiles. Due to their large apertures, geogrids may interlock with base course aggregate if there is an appropriate relationship between geogrid aperture size and aggregate particle size. While the degree of interlocking depends on the relationship between geogrid aperture size and aggregate particle size, the effectiveness of interlocking depends on the in-plane stiffness of the geogrid and the stability of the geogrid ribs and junctions. As a result of interlocking, the mechanisms of unpaved structure reinforcement are different for geotextiles and geogrids (Giroud and Han, 2004a).

The review of the significant work on design methods indicates four original works that have contributed substantially to a better understanding of geosynthetics used in roadway applications (Barenberg et al., 1975; Steward et al., 1977; Giroud and Noiray, 1981; Houlsby and Jewell, 1990; Giroud and Han, 2004a and 2004b). In analytical methods, it is assumed that all the rut depth is developed in the subgrade and, the base moves as a block. This assumption is correct for all practical purposes, where the foundation soils are low resistance, and the thickness of the base layer is thin. Based on the theory of plastic equilibrium, the ultimate bearing capacity q_{lim} for soils in this condition is (for a zero base thickness):

$$q_{\lim} = (2+\pi)c \tag{1}$$

Where, c represents the cohesion of the soil. However, the localized plastic strains, which may cause, in any manner, the localized failure, begin towards the elastic limit (for a zero base thickness), given by:

$$q_{\lim} = \pi c \tag{2}$$

The failure mechanism of the clay soil, assumed at 45° in the plastic zone, is shown in Figure 1. For a given base thickness, the pressure limit on the subgrade is given by:

$$q_{\lim soil} = mN_c c_u \tag{3}$$

Where m, represents, for the authors, the bearing capacity mobilization coefficient, N_c is the bearing capacity factor of the subgrade. C_u is the undrained shear strength of the subgrade. The authors take for N_c, tan β, and m, the values listed in Table 1.

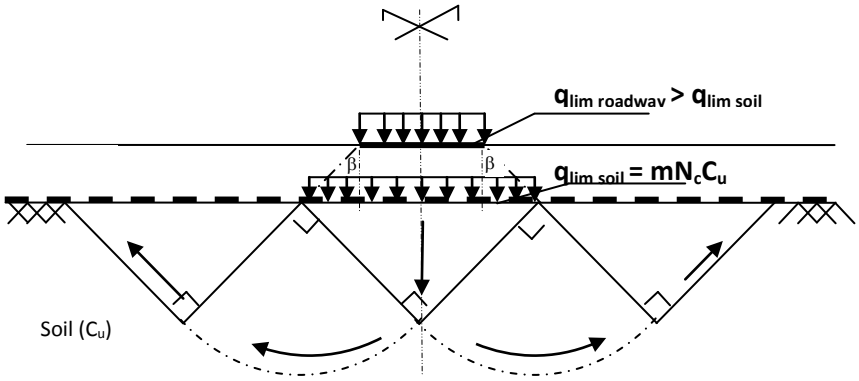

Figure 1: Failure mechanism

Table 1. Values of N_c, tan β and m according to different authors

Authors	Value of N_c			tanβ	m
	Without Reinforcement	With Geotextile	With Geogrid		
Barenberg et al., 1975	3.3	6.00	-	According to Boussinesq	1
Steward et al., 1977	2.8	5.0	-	According to Boussinesq	1
Giroud and Noiray, 1981	3.14	5.14	-	0.6	1
Houlsby and Jewell, 1990	3.07	5.69	-	To choose arbitrarily	1
Giroud and Han, 2004	3.14	5.14	5.71	computable	≤1

Perkins and Ismeik (1997) provide an overview of the majority of experimental studies and numerical analysis, which were conducted on reinforced pavements. Full scale and laboratory scale experimental work carried out until now, show an improvement especially in the rut depth, and substantial gain in the thickness of the pavement. However, these experimental results taken by themselves seem to be insufficient for the development of a recognized process design due to many dependent variables influencing the problem. Moreover, varying degrees of success have been made in the development of finite element models to predict the response of reinforced flexible pavements.

This work deals with numerical simulation using Flac software, to investigate the improvement of the bearing capacity of reinforced unpaved roads over soft clay. The mechanism by which the reinforcement improves the behavior of the roadway under the effect of a static single load is examined. The unpaved road is subject to the

application of a single static load. Although in reality the loading may be over a rather complex area, it was idealized here as a strip loading (plane strain) and the pressure-displacement behavior was determined for small and large strain analysis for unpaved roads with or without reinforcement.

Numerical Simulation with Flac Presentation of the case study

The case study consists to analyze the behavior of a roadway under the effect of a single static load. The roadway, considered here, is an unpaved road that can accept deformations in the form of ruts, which can reach 100 mm, and more. The roadway is considered as a two layer system, consisting of a base layer, made in, selected material, resting on a low bearing capacity soil. The behavior of the roadway, which may be reinforced or not by geogrid, arises, as a plane strain problem of determining the bearing capacity of a shallow strip footing resting on a two-layer soil. Indeed the permanent deformation of the road in the form of a rut justifies the assumption of plane strain.

The problem is formulated, in large strain, to represent the deep ruts that can develop, and are allowable, on unpaved roads. Contacts soil-geogrid and geogrid-base are governed by an interface that has a behavior, elastic perfectly plastic of Mohr-Coulomb. Given the symmetry about the vertical axis, and considering a half-width of foundation, B= ½ a = 0.159 m, the boundary conditions can be presented as shown in Figure 2.

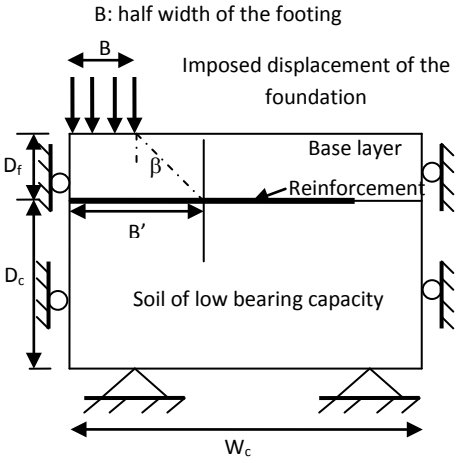

Figure 2: Case Study

Electronic discourse within computer mediated virtual courses supports conversations of practice and learning. The loading of the roadway structure is achieved by imposed displacement of the load until a final displacement, called rut, limited in this work at $\delta = 0.8\ B = 0.8x0.159 = 0.127$ m is reached. It is assumed that beyond this rut depth, the roadway becomes impractical. Therefore the pressure of the foundation necessary to achieve this displacement is considered as the ultimate pressure. The physical and mechanical properties of the materials used are as follows:

Subgrade: E =10 MPa, $\nu = 0.33$, $\rho = 1900$ kg/m3, $C_u = 30$ KPa, Dc = 2.54 m = 16B, W_c =3.18 m = 20B.

Base: E = 50MPa, $\nu = 0.25$, $\rho = 2200$ kg/m3, $\varphi = 40°$, C = 0., $\psi = 20°$, D_f = 0,212m.

Geogrid: E =146 MPa, $\nu = 0.33$.

Interface Soil/geogrid and base/geogrid: kn = ks = $5x10^9$ N/m3, φ=35°, C=0., kn and ks are respectively the normal stiffness and shear stiffness of the interface element.

E, ν, ρ, C_u, φ, ψ, C have the usual meanings, i.e. respectively: elastic modulus, Poisson's ratio, bulk density, undrained shear strength, friction angle, dilation angle and cohesion.

Numerical Analysis with Flac

The plane strain analysis is developed using the software Flac (Fast Lagrangian Analysis of Continua (Flac), 2000). The corresponding mesh is shown in Figure 3. To achieve a final rut (displacement) of $\delta = 0.8B = 0.8x0.159 = 0.127$ m, a downward velocity is imposed to the 4 gridpoints representing the footing. A constant velocity of $-2.5x10^{-6}$ m/step is adopted for the case of a non-reinforced roadway and a velocity of $-1x10^{-6}$ m/step for a reinforced roadway. These velocity values were retained after several preliminary simulations.
The geogrid was modeled as a structural beam, as defined by Flac (2000). The beam adopted has zero inertia, to characterize the membrane effect of the geogrid.

Simulations results and analysis in small and large strains

Load-displacement simulations

The results presented in Figure 4, show the load-displacement simulation of the 4 possible cases, unreinforced road in small strain (BF40C30S), unreinforced in large strain (BF40C30), reinforced in small strain (BF40C30RS) and reinforced in large strain (BF40C30R).

Regarding the improvement in bearing capacity of the structure, provided by the reinforcement, and according to the results obtained with Flac simulations, the improvement is about 29% for small strain analysis (BF40C30S and BF40C30RS simulations). The equivalent analysis in large strain (BF40C30 and BF40C30R simulations) shows an improvement of 46% in bearing capacity. This demonstrates that the reinforcement has a better effect on increasing the bearing capacity of a two-layer system, in large displacement.

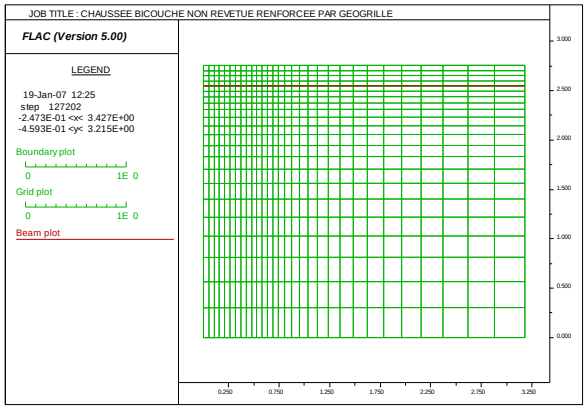

Figure 3: Mesh geometry

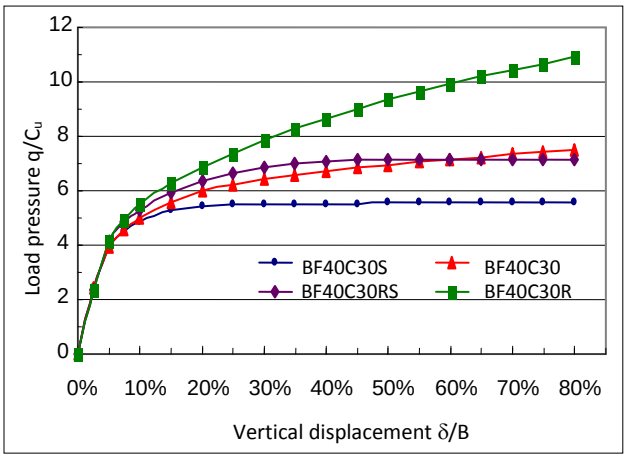

Figure 4: Pressure-Displacement

Tangential stresses acting on the interface soil-base

The analysis of the tangential stresses in figure 5 shows that for an unreinforced roadway the maximum shear stress reached is $\tau = 1.C_u$. on the contrary, for a reinforced roadway, one can note that the geogrid causes the increase of tangential stresses on the upper side of the geogrid, which explains the lateral confinement provided by the geosynthetic, Burd and Brocklehurst (1990). However the stresses are reduced by the reinforcement to a value of $\tau = 0.4\ C_u$ on the subgrade. This shows the effect or the mechanism of reinforcement.

Parametric Study

Effect of the Reinforcement Stiffness on the bearing capacity

Figure 6 shows the variation of the ultimate pressure, with the variation of the geogrid stiffness. We can note the net evolution of the bearing capacity with the increase of the geogrid stiffness. But this improvement, reaches a limit for the stiffnesses exceeding J =1000 KN/m.

Effect of the Stiffness of the Reinforcement on the maximum tension in the geogrid

Figure 7 shows the variation of the maximum tension in the geogrid with the variation of the stiffness of the geogrid. We can note the evolution of the maximum tension with the increase of the stiffness of the geogrid. It can also be noticed that beyond a stiffness of J = 1000 KN/m, the maximum tension in the geogrid continues to increase without any counterparty on the bearing capacity. Therefore, one can conclude that there is an interest to study the ratio stiffness / bearing capacity in order to fix the choice of an optimal geogrid.

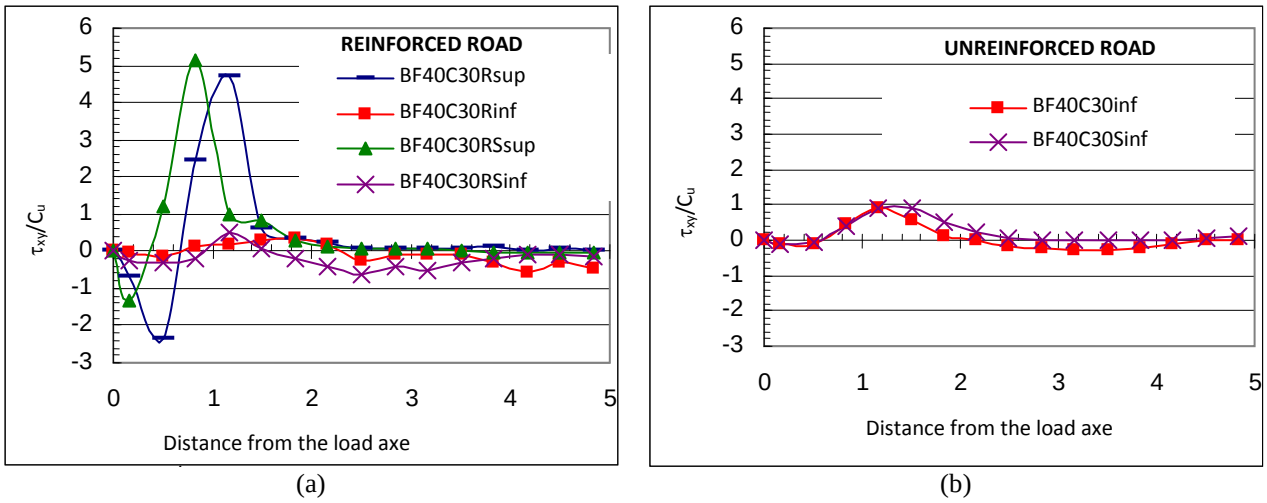

(a) (b)

Figure 5: Tangential Stresses acting on the interface soil-base: (a) reinforced road; (b) unreinforced road; sup = upper side of the geogrid; inf = lower side of the geogrid

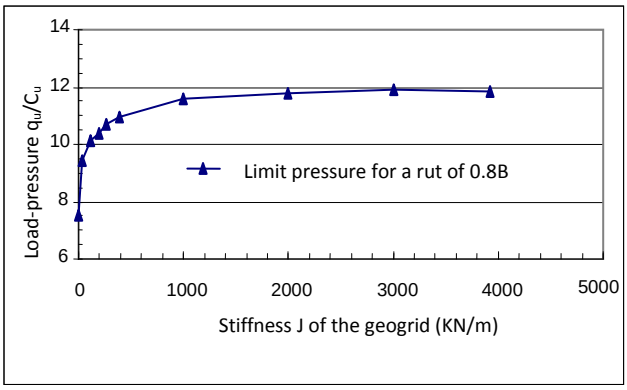

Figure 6: Effect of the stiffness J of the geogrid on the bearing capacity

Effect of the undrained cohesion C_u of the soil supporting on the bearing capacity

Figure 8 shows the expression of the ratio of the ultimate pressure with reinforcement on the same pressure without reinforcement. One notices that the improvement of bearing capacity is higher for soils with low resistance. Indeed the improvement of bearing capacity is 58% for a soil of C_u = 15 KPa, but only 35% for a soil of C_u = 60 KPa.

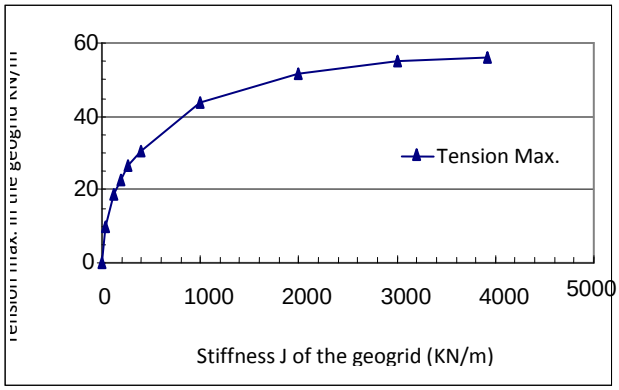

Figure 7: Effect of the stiffness J of the geogrid on the maximal tension on the geogrid

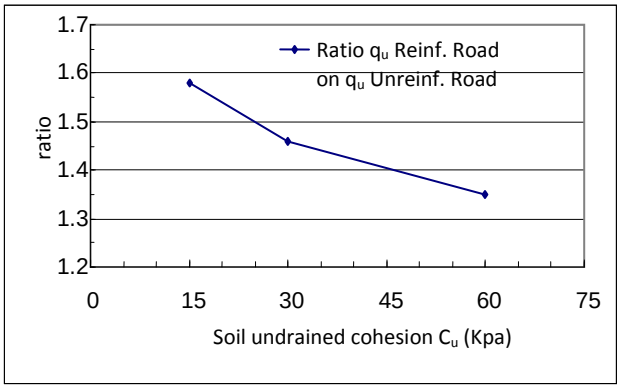

Figure 8: Effect of the soil strength (C_u) on the improvement of the bearing capacity

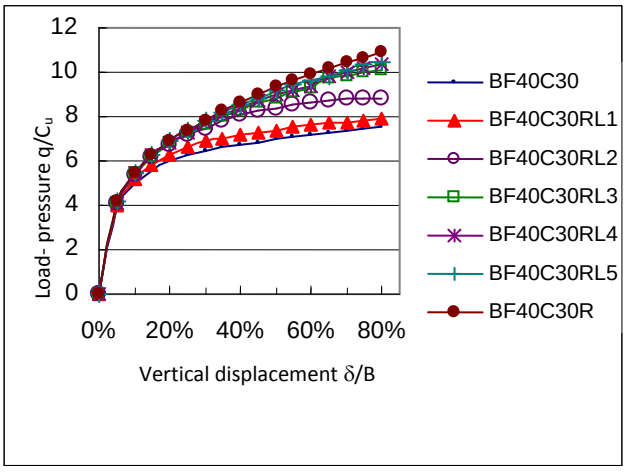

Figure 9: Effect of the anchorage length on the pressure-displacement behavior. Lengths of reinforcement: L1=0.94 B; L2=1.67B; L3=2.17B; L4=2.83B; L5=4B; R=20B

Effect of the anchorage length on the pressure-displacement behavior

Figure 9 shows the pressure-displacement behavior, for seven, different variants, an unreinforced road, a reinforced road, with the anchoring lengths L1 to L5 ranging from 0.94B to 4B and, a basic variant with reinforcement over the entire width of the road. One can notice that an anchoring of L4 = 2.83 B can mobilize a bearing capacity equal to 95% of that mobilized by the same geogrid, anchored on, the entire width of the road.

Conclusions

By analyzing the results of the simulations carried out in this research with the FLAC software, we can conclude the following:

- The large strain simulations show more improvement, in the bearing capacity and, follow better the actual behavior.
- The parametric study on the effect of the stiffness of the reinforcement helps to distinguish two zones: a zone of low stiffness characterized by high sensitivity of the bearing capacity and a zone of high stiffness characterized by an attenuating sensitivity with the increasing of the stiffness. This study explains the conflicting opinions in the literature on this point.
- The maximum tension in the geogrid continues to increase proportionally with the increase of the stiffness without counterparty in the bearing capacity. This raises the interest of the study of the ratio stiffness / bearing capacity for an optimal choice of a geogrid.
- The study shows that the improving of the limit pressure is inversely proportional to the undrained cohesion of the soil.
- The study shows that the length of the reinforcement should be just sufficient enough to mobilize the mechanism of reinforcement.

References

Barenberg, E. J., Hales, J., and Dowland, J. (1975). Evaluation of Soil-Aggregate Systems with MIRAFI Fabric. *Report No. UILU-ENG-75-2020, prepared for Celanese Fibers Marketing Company.* University of Illinois.

Burd, H. J., and Brocklehurst, C. J. (1990). Finite Element Studies of the Mechanics of Reinforced Unpaved Roads. *Proceedings of the Fourth International Conference on Geotextiles, Geomembranes and Related Products, Balkema,* Vol. 1 (pp 217-221). The Hague, Netherlands.

FLAC (2000) – Fast Lagrangian analysis of continua, *Itasca Consulting Group, Inc.*, Minneapolis, MN.
Giroud, J. P., and Noiray, L. (1981). Geotextile Reinforced Unpaved Road Design. *Journal of the Geotechnical Engineering Division, ASCE,* Vol. 107, No. GT9 (pp 1233-1254).

Giroud, J. P., and Han, J. (2004). Design method for geogrid-reinforced unpaved roads. I: Development of design method. *J. Geotech. Geoenviron. Eng.*, 130(8) (pp 775–786).

Giroud, J. P., and Han, J. (2004). Design method for geogrid-reinforced unpaved roads. II: Calibration and applications. *J. Geotech. Geoenviron. Eng.*, 130(8) (pp 787–797).

Houlsby, G. T., and Jewell, R. A. (1990). Design of Reinforced Unpaved Roads for Small Rut Depths. *Proceedings of the Fourth International Conference on Geotextiles, Geomembranes, and Related Products, Balkema*, Vol. 1 (pp 171-176). The Hague, Netherlands.

Perkins, S.W. and Ismeik, M. (1997). A Synthesis and Evaluation of Geosynthetic-Reinforced Base Layers in flexible Pavements: Part I and Part II. *Geosynthetics International*, Vol. 4, No. 6 (pp 549-621).

Steward, J.E., Williamson, R., and Mohney, J. (1977). Guidelines for the use of Fabrics in Construction of low – Volume Roads. *Report N° FHWA – IS – 78 – 205, Pacific Northwest Region Forest Service, US.* Departement of Agriculture, Washngton, DC, USA, 172 p.

Performance of different types of FRP sheets bonded to concrete using flexible adhesive

Hesham M. Diab

Civil Engineering Department, Assiut University, Egypt
heshamdiab2@yahoo.com

Abstract: De-bonding problems stand as a critical barrier against a wide range of usages of FRP composites in structural strengthening and repairing applications. Results of an experimental campaign on FRP-concrete debonding are presented in this study. Specimens with different types of FRP sheets bonded to concrete prism using flexible adhesive were conducted to determine the effective bonding length and ultimate bond capacity of FRP-concrete interface. The experimental results from double lap shear specimens indicated that the flexible adhesive has increased both of the effective bonding length and the ultimate bond capacity of FRP-concrete interface. Increase of fracture energy of FRP-concrete interface has been clearly observed due to flexible adhesive for all different types of FRP sheets. Analytical models available in the literature were adopted to evaluate the bond strength and the effective bond length of the experiment results in this study. Consequently, the existing models need to be modified to consider the type of adhesive layer. A unique feature of the present study is that a simple modification done to the most popular bond strength model, Chen and Teng model (2001), to predict both bond strength and effective bonding length considering the type of adhesive layer. The validation of bond strength model is supported via experiment test results.

Key words: Bond strength model, Flexible adhesive, FRP sheet, Concrete.

Introduction

External bonding of FRP sheets/plates is an effective and popular method for the rehabilitation of reinforced concrete structures. The mechanical performance, including the strength of the external bonded FRP structural system, is often determined by the bond between FRP composites and concrete. The bond interface, FRP-concrete interface, is usually the weakest link, and debonding at the interface is usually the critical failure mode. Debonding initiation in beams strengthened with FRP composites generally take place in regions of high stress concentration at the concrete-FRP interface. These regions include the ends of the FRP reinforcement, and those around the shear and flexural cracks (Buyukozturk et. al. 2002). Figure 1 shows the fundamental debonding mechanisms that may result in premature failure of FRP strengthened beams. Thus, determination the bond capacity of the FRP-concrete interface is an important subject, and has attracted extensive research till now (Caggiano at. al. 2012, Wu at. al. 2012, Wu at. al. 2012, Tuakta and Büyüköztürk 2012).

Based on the extensive tests, researchers concluded that bond capacity is affected mainly by mechanical and physical properties of concrete, thickness and stiffness of the FRP, thickness of the adhesive, and the bonded length (Chen & Teng 2001, Neubauer & Rostasy 1997, Wu at. al. 2009). However, some researchers concluded that thickness of the adhesive has negligible effect on mean and peak shear stresses (Hamoush and Ahmed 1990, Nakaba at. al. 2001). Analytical models have been proposed in order to predict the behaviour and the ultimate bond strength of the FRP-strengthened system. It is interesting to note that most of the existing models, which are in reasonable agreement to experimental results(Chen & Teng 2001, Neubauer & Rostasy 1997, Wu at. al. 2009), neglect the adhesive layer properties.

Indeed, a number of researchers investigated the effect of flexible adhesive on the bonding of FRP sheets (Xia & Teng 2005, Dai at. al. 2005). Dai et. al.(2005) provided a summary report on the flexible bonding system. The contents included the bond characteristics of FRP/concrete joints, strength and ductility of FRP strengthened